Petrology, Geochemistry, Petrogenesis and Reactivation of Volcanic Tuffs at Dair El-Kahif Area, NE-Jordan

Ibrahim A. Bany Yaseen [1)✉], *Zayed Al-Hawari* [2)] *and Abdullah A. Diabat* [1)]

[1)] Institute of Earth and Environmental Sciences, Al-al-Bayt University, Al-Mafraq, Jordan
✉ Corresponding author, E-mail: ibanyyaseen@Yahoo.com
[2)] Department of Environmental and Applied Geology, Faculty of Science, University of Jordan, 11942, Amman, Jordan

ABSTRACT

The volcanism in the western Arabian plate extends from the Red Sea through the Harrat Ash-shaam system to western Syria. The aforementioned volcanic activity produced large quantities of alkali olivine basalts and tuffaceous materials. The stratovolcano (7km) NE of Dair El-Kahif, NE Jordan has been investigated. The results show that dominant mineral phases are olivine, augite, plagioclase, magnetite and ilmenite. Chemical analysis of the whole rock tuff samples confirms alkali olivine magma origin. Low concentrations of Li and Rb in tuff samples are used as an argument against the contamination of the basaltic magma during its journey to the surface. The MgO and Mg-values ($Mg/Mg+Fe^{2+}$) in samples from volcanic tuff exhibit different degrees of fractionation, which are indicated by the varying concentrations of incompatible trace elements (Ba, Rb, Sr). The thermometric evaluation of tuff determined by using pyroxene thermometers revealed a temperature range between 1022-1083°C and a pressure of 5-10 kbars. The low Mg-ratio ($Mg/Mg+Fe^{2+}$) is due to fractional crystallization of olivine and pyroxene in tuff samples. The variations of incompatible elements imply derivation from a peridotite source in the upper mantle with low degree of melting (<20%). The volcanic activity took place in phases corresponding to rifting associated with the sinistral movement along the Dead Sea Transform and the later reactivation processes.

KEYWORDS: Volcanic tuff, Megacrysts, Partial melting, Arabian plate, Fractionation, Alkali basaltic magma, Reactivation.

INTRODUCTION

The structural pattern of Jordan has been affected by the opening of the Red Sea and Gulf of Aden; thus the lateral movement of the Arabian plate towards north along the Dead Sea Transform fault (Fig. 1). The Dead Sea Transform, also named Rift, is a 1100 km long sinistral fault system that connects the Gulf of Aqaba-Red sea spreading system to the convergence zone in the Taurus-Zagrous Mountains (Fig. 1). In terms of

plate tectonics, it is considered a plate boundary between the Arabian plate in the east and Palestine-Sinai sub-plate (part of the African plate) in the west. The Dead Sea Transform (DST) is the major tectonic feature controlling the stratigraphic and structural evolution of the region since the Miocene.

The structure and the deformation of the region have been the focus of many discussions and interpretations. The tectonic deformation of the region has been attributed to N-S relative motion along the Dead Sea Rift (e.g. Quennel, 1959; Freund, 1965). Because of its key position in the geology of the region, the Dead Sea

Rift region and its margins have been the subject of many detailed mapping and regional structural studies (e.g. Picard, 1943; Quennel, 1959; Freund, 1965, 1970; Bender, 1968; Garfunkel, 1970, 1981; Garfunkel et al., 1981; Eyal and Reches, 1983). Comprehensive structural studies were based on small- scale or mesostructures (e.g. Reches et al., 1981; Eyal and Reches, 1983; Ron and Eyal, 1985; Eyal, 1985; Eyal, 1996; Diabat, 1999; Zain Eldeen et al., 2002; Diabat et al., 2004), and on focal plane solutions of earthquakes

(e.g. Ben Menahem, 1979; Badawy and Horvath, 1999). The Dead Sea Fault System (Fig. 1) is important because it is the Arabia-Africa plate boundary and so records the motion between these plates. It consists of left-lateral fault segments that connect the active oceanic spreading centers in the Red Sea to the compressional deformation zones in southeast Anatolia and the Zagros (Garfunkel, 1981). It has a total length of 1100 km, and formed in regions of overlap between left-stepping and right-stepping fault segments.
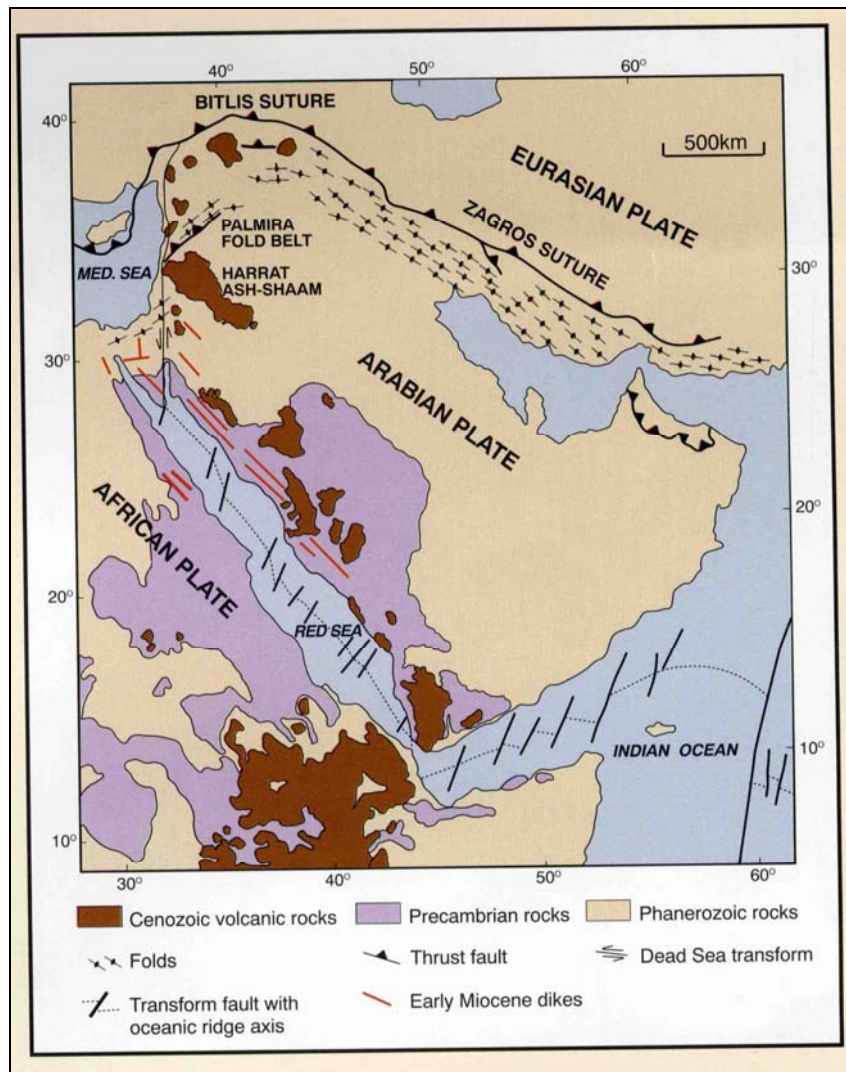

Figure 1: Regional tectonic map showing the location of volcanic fields in the Arabian plate
(after Camp and Roobol, 1989)

The Dead Sea Transform fault (DST), a 1100 km-long major plate boundary accommodates most of the active deformation between the Arabian and African-Sinai plates. Taking the historical seismicity of the region into account (Abou Karaki, 1987; Ambraseys et al., 1994; Sbeinati et al., 2005), the fault was likely the source of several large earthquakes (M >7) with severe damage, surface faulting and landscape changes (Ferry et al., 2007). Slip rates along the DST vary from 2 to 10 mm /yr (e.g. Garfunkel et al., 1981; Galli, 1999; Niemi et al., 2001).

GPS data indicate 6mm/yr of relative Arabia/Africa motion in the northern Arabian platform. During Cenozoic times, basaltic lava poured from vertical fissures and local vents along the Jordan rift, mountain ridge in central Jordan and in north eastern Jordan (Fediuk and Al-Fugha, 1999). They are part of the Arabian plateau basalt which covers large areas in Saudi Arabia, Jordan and Syria. The Cenozoic volcanism in northeastern Jordan (Harrat, within an area of 11,400km²) has a relatively long period of magmatic sequence extending from the Oligocene to the Holocene (Barberi et al., 1979, Moffat, 1988; Duffield et al., 1988; Ilani et al., 2001). The extensive volcanism in Jordan was extruded intermittently with the Jordan-Dead Sea Rift and other faulting episodes. Previous petrochemical studies on the NE basaltic plateau revealed alkali basalts (e.g. Barbara et al., 1979; Moffat, 1988; Saffarini et al., 1985; Al-Malabeh, 1994; Al-Malabeh et al., 2002; Shaw et al., 2003; Ibrahim and Al-Malabeh, 2006).

The studied area is located within Harrat Al-Shaam, at the western margin of the Arabian plate, about 7km NE Dair El-Kahif at 32° 21′ 12″ N and 36° 08′ 123″E (Fig.2), tectonically controlled by the Arabian plate movement, which moved northwards along the Dead Sea Transform fault .The other volcanic tuff is located at the north eastern side of the Dead Sea area (Barberi et al., 1979).

The volcanic activity in north-eastern Jordan was formed in the time of rifting process along the Jordan Rift. The tuffs are characterized by bulk chemical and petrographical homogeneity. In north-eastern Jordan Rift zone, many rather small areas of basalt and tuff were mapped (Bender, 1968; Al-Malabeh, 2003). The volcanic tuff is of Pleistocene age (Barberi et al., 1979; Bender, 1968). The structure of the volcanic tuff is presented along with the petrology of different inclusions of sedimentary rocks in the pyroclastic and basaltic bombs. The nature and magmatic differentiation trends of the alkali olivine basalts in NE Jordan were fully studied. However, very little emphasis was put on the tuffaceous material associated with these basalts.

The purpose of this study is to describe the occurrence of the tuff in NE volcanoes and to shed light on their mineralogy, geochemistry and mode of origin. Because there are no previous studies which dealt with paleostresses in this area (Harrat Al-Shaam), the present study is an attempt to determine the principal stress axes, the maximum horizontal shear and the related stress fields based on fault- slip data of mesostructures.

GEOLOGICAL SETTING

In northeastern Jordan (Fig. 2), basalts cover an area of approximately 11,000 km² and extend along the east side of Al-Azraq-Wadi As-Sirhan basin (Bender, 1974). Seven known different phases of major volcanic activities in north eastern Jordan were investigated based on both field observations and borehole data (e.g. Ibrahim, 1993, 1996; Tarawneh, 1999a,b). The lower three phases are known only from wells drilled for groundwater in Wadi Dhuleil, northeast of Amman, the thickness of these flows reaches 150m, the upper four phases are exposed at the surface between oil pump stations H-5 and H-4 in the central part of the northeastern Jordan plateau.

The volcano under consideration is of strato - volcano type (Al-Fugha, 1993), and is situated 7 km NE Dair El-Kahif (Fig. 2). It rises above the surface of the basalt flow by 120 m. The wall boundary of the volcano has gentle slopes, with fine grained ash, angular and spherical pyroclasts of diameters less than 0.3 cm. Basaltic bombs in different sizes, ranging in diameter between 0.5 and 2 m, are exposed (Fig. 3), and basaltic layers of blocky lava with an average thickness of 0.5m, are also present.
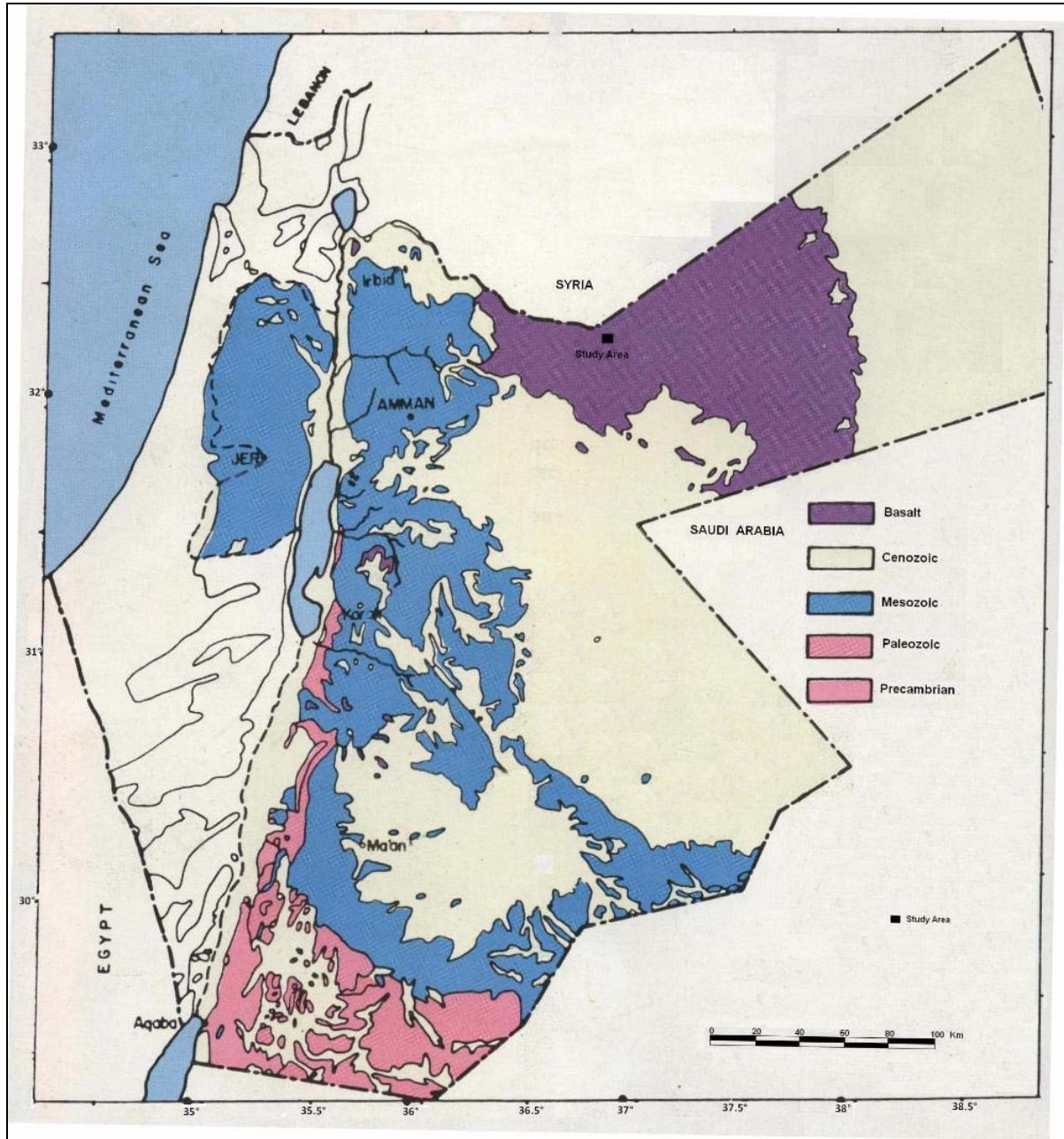
Figure 2: Geological map of Jordan showing the location of studied volcano area (after NRA, Jordan)

Jordan is part of the Arabian plate. The Dead Sea Rift forms the western boundary of the Arabian plate, which is drifting towards the Tauros-Zagros compressional zone. Uplift and tensional depressions parallel to the Red Sea are developed and the most important one is the NW-SE striking Azraq - Sirhan graben structure. The volcano is aligned NNW-SSE and is situated on the eastern side of a major fault trending NNW-SSE (Fig.2).
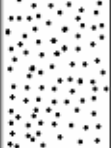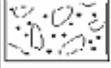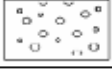
section	Thick m	Lithological Description
	3-6	Lava- bombs of more than 1m diameter and fine grained lapilli.
	5-6	Lava-bombs (0.5 to 2.0m diameter) with some fine grained lapilli.
	6	Alternating layers of fine lapilli-tuff (grain size 1/2cm and coarse tuff (grain size 2/8cm).
	1-2	Welded lapilli and lava bombs of 30cm diameter
	8-10	Coarse grained lapilli (1-3 cm diameter) and fine volcanic material (1/2 cm diameter)

Lava-bombs and fine grained lapill

Fine grained lapilli   Coarse grained lapilli

Figure 3: Type section of tuff-sequences in the studied area

METHODOLOGY

Method of Stress Inversion

The inversion is based on Bott's (1959) assumption that slip on a plane occurs in the direction of the maximum resolved shear stress. The slip direction on the fault plane is inferred from frictional grooves or striations. The data used for the inversion are the fault plane, slip line orientation and the sense of movement on each fault plane. The fault-slip data are inverted to obtain the four parameters of the reduced stress tensor as defined in Angelier (1979, 1989 and 1991): the principal stress axes; $\sigma1$ (maximum compression), $\sigma2$ (intermediate compression) and $\sigma3$ (minimum compression) and the ratio of principal stress differences R= $(\sigma2 - \sigma3)/ (\sigma1- \sigma3)$ (Fig.5). The four parameters are determined by using successively an improved version of the Right Dihedral method of Angelier and Mechler (1977), and a four- dimensional numeric rotational optimization method (Delvaux, 1993; Delvaux et al., 1997) (Fig. 5). The analysis of paleostresses based on mesostructures or minor faults in terms of fault-slip data is a good way to reconstruct stress tensors and the related stress field.

Sampling and Analytical Techniques

Eleven samples were collected from upper, middle and bottom parts of the tuff section. Minerals were

analyzed using EMX-ARL electron microprobe at the Institute of Mineralogy at the University of Tuebingen (Germany), using the factor of Bence and Albee (1968). The chemical analysis for major and trace elements of

the whole rock samples was carried out using the atomic absorption spectrophotometer at the University of Jordan. Thin sections were prepared for each sample.
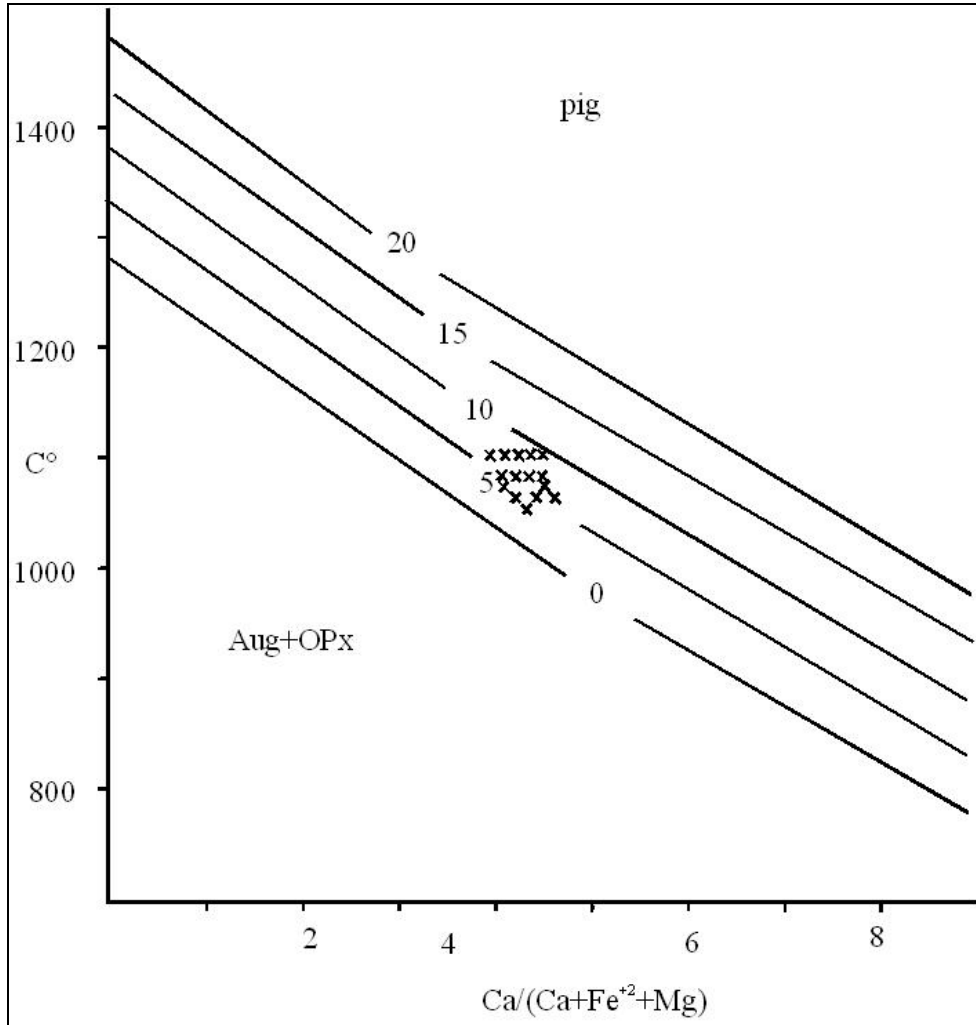
Figure 4: The Ca/(Ca+Fe^{+2}+Mg) content of augite as function of pressure and temperature (after Lindsley, 1983)

RESULTS

Paleostresses

The paleostress analysis indicates that $\sigma 1$ (SHmax) and $\sigma 3$ (SHmin) are sub-horizontal and $\sigma 2$ is sub-vertical in one stress tensor (Fig. 5a), belonging to the strike-slip regime. It shows NW-SE compression and

NE-SW extension. This direction reveals a regional stress regime rather than a local stress regime; i.e it is considered as a regional DSS. This stage of deformation took place in Miocene/ Pleistocene (see Eyal, 1996; Eyal and Reches, 1983; Zain Eldeen et al., 2002; Diabat, 1999; Diabat et al., 2004).

a

weighed
S LOWER
n = 12

⊙ õ1: 08/310: 53 x 0
▲ õ2: 78/179
◉ õ3: 09/041: 65 x 100
R, CD%: .5 22.9 ±4.6
Pure STRIKE-SLIP

CD %

60

30

0

0   frequency x weight   8

b

weighed
S LOWER
n = 8

⊙ õ1: 72/256: 131 x 0
▲ õ2: 04/155
◉ õ3: 18/064: 130 x 100
R, CD%: .37 12.5 ±2.4
Pure EXTENSIVE

CD %

60

30

0

0   frequency x weight   10

→

- 342 -
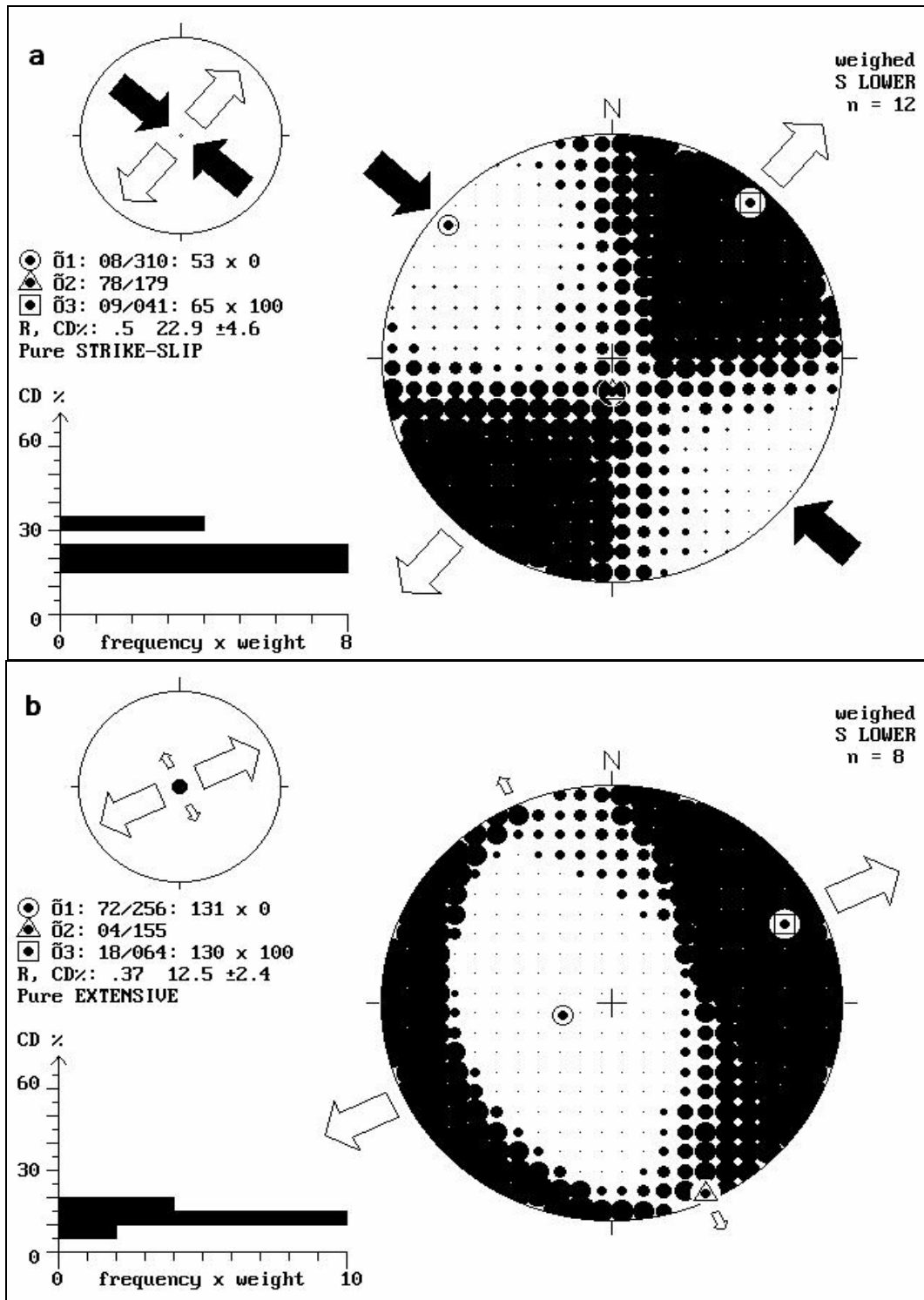
Figure 5: The paleostress tensors showing the directions of compression and tension, the SHmax and SHmin, which reflect the reactivation stresses in the study area
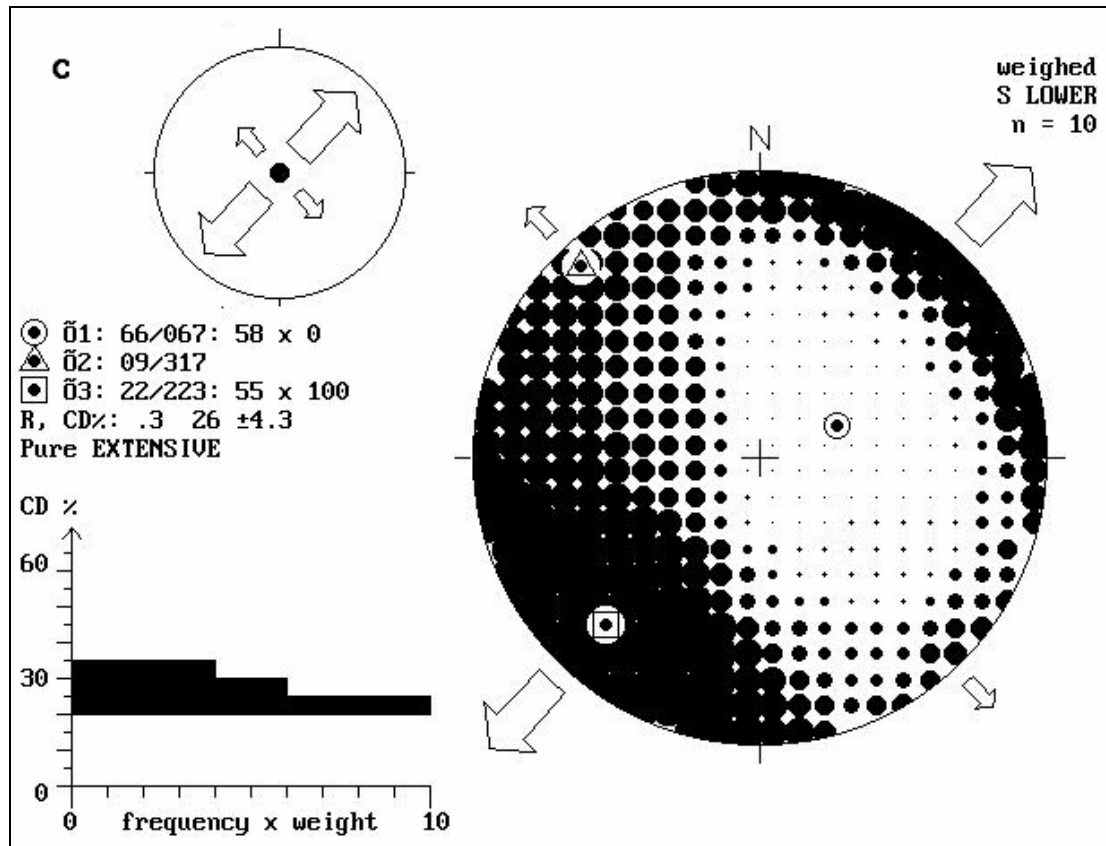
The other two tensors, (Figs. 5 b and c), show a pure- extensive regime in which $\sigma1$ is sub-vertical, reflecting the reactivation processes as normal faulting of the strike-slip faults (this is also shown by the superimposed sub-vertical slickensides on sub-horizontal slickensides). They show an extension in a general trend swinging around NE-SW. This direction is perpendicular to the Red Sea axis (Fig. 1).

Petrology

The volcanic tuff consists mainly of coarse-grained lapilli and fragmentary materials with diameters of less than 0.5cm. The materials consist of angular and subangular vesicular lava pieces, which are locally welded.

A distinction can be made between ellipsoidal unipolar, spindle shaped and twisted shaped bombs. Occasionally, sedimentary materials (limestone boulders) have been thrown out. Petrological work showed that the tuff is composed of olivine, clinopyroxene, plagioclase, magnetite and ilmenite. The average modal composition is 49 vol% plagioclase, 25 vol% clinopyroxene, 21 vol% olivine and 5 vol% magnetite and ilmenite.

Olivine occurs as pale-yellow euhedral to subhedral crystals with an average size of about 0.5 mm. Augite is colorless or pale brown to pale green and occurs as euhedral phenocryst 1-4 mm in length. It shows a strong zonation and a good cleavage. The groundmass augite shows prismatic crystals. Some augite crystals

encompass olivine and ore inclusions. Plagioclase occurs as hypidiomorphic laths, which form in some samples an ophitic structure. It varies in grain size from 0.2- 0.5 mm. It also occurs in the groundmass in an intergranular pilotaxitic and microcrystalline form. The plagioclase laths have a composition of An_{50-60} (Labradorite), and extinction angles on plagioclase crystal range from 28° to 32°. Magnetite and ilmenite crystals, with vitreous luster, are euhedral to subhedral and range from 0.3-0.5 mm in diameter.

Mineral Chemistry

Tables (1, 2, 3 and 4) show the mineral chemistry of olivine, clinopyroxene, plagioclase, magnetite and ilmenite, respectively.

Olivine: The forsterite content of the olivine grains from eleven samples as listed in (Table 1) ranges from 71.4-82.5%. Average calcium concentrations of olivines are 0.24% with a rather homogeneous distribution except sample No. 5. The high value could be explained by diffusion from neighboring clinopyroxenes. The SiO_2 content shows minor variation. The XFe/XMg ratio in olivine is 0.1. The ($Mg/Mg+Fe^{2+}$) ratios range from 0.79-0.82 at a constant temperature, which could indicate a mantle homogeneity. The average concentration of manganese is 0.30% and the correlation with fayalite content is only very weak. No variation in the olivine composition is noticed between the tuff samples.

Clinopyroxene: The clinopyroxene chemical results are listed in (Table 2) and can be described as titaniumaugite. The (Ca/Ca+Mg) ratios are 0.54 -0.59. The molecular proportions of $CaSiO_3$, (Wo) $MgSiO_3$ (En) and $FeSiO_3$ (Fs) of clinopyroxene give an average composition of (Wo50.4, En32.6, Fs17.0). The clinopyroxenes are relatively Ca rich and mainly Fe-poor. Zonation in clinopyroxene as indicated by chemical heterogeneity with respect to Cr and Al is observed. The average Al, Cr, Na and Ti abundances are 6.1, 0.61, 0.04 and 2.93%, respectively.

Plagioclase: The chemical analysis of plagioclase (Table 3) shows that it has a composition of An = (50-60%). The plagioclase composition exhibits variations in total SiO_2 (51.92 - 54.63) and Al_2O_3 (28.31-30.59) contents. The average Ca concentrations are 11.70% and the average Na-concentration is 4.54%. These data are correlated with that of Labradorite from Millard, Utah with 12.28% CaO and 4.21% Na_2O (Fediuk and Al-Fugha, 1999). The CaO and Na_2O show variations and could be explained by the equilibrium conditions during their crystallization.

The plagioclase series normally contains a certain amount of orthoclase molecule, $KAlSi_3O_8$ with an average of 0.37wt% K_2O in Labradorite. This value tends to increase gradually towards the sodic end of the plagioclase series. Other oxides present in plagioclase in very limited amounts include FeO, MnO and TiO_2.

Magnetite and **ilmenite** grains were analyzed (Table 4). The major elements were Fe and Ti. Magnetite has a relatively lower iron content through the chemical composition and is considered as titanomagnetite.

DISCUSSION

Field observations and tuff materials indicate that several eruptions took place starting with lapilli and ending with coarse components. The chemical analysis of tuff samples (Table 5a) proved that it is undersaturated with respect to silica content. According to the petrological study and CIPW norm calculations in Table (5b), the studied tuff belongs to the alkali basaltic magma. Chemical variations indicate that Mg rich samples are rapidly crystallized and have a greater solid solution towards Ca end member. The clinopyroxene with the larger $MgSiO_3$ proportions in solid solution is equilibrated under higher temperature (Wilson, 1989).

The investigated volcano resulted from magma rich in volatile constituents lost explosively from a fissure like eruption, and magma produced NE volcano.

The MgO and Mg-values ($Mg/Mg+Fe^{2+}$) exhibit different degrees of fractionations as indicated by the varying concentrations of incompatible trace elements Ba, Rb and Sr (Table 5c).

Table 1: Microprobe analysis of olivines in wt%

Sample No.	1	2	3	4	5	6	7	8	9	10	11
SiO_2	38.88	38.45	39.06	37.95	37.83	38.18	38.72	37.66	38.91	38.25	38.38
TiO_2	0.00	0.00	0.00	0.00	0.22	0.13	0.00	0.00	0.00	0.00	0.00
Al_2O_3	0.00	0.00	0.00	0.00	0.58	0.00	0.00	0.00	0.00	0.00	0.00
Cr_2O_3	0.00	0.00	0.00	0.00	0.00	0.00	0.00	0.00	0.00	0.00	0.00
FeO	17.61	18.47	16.55	20.39	25.12	19.86	17.06	21.61	20.26	19.28	18.94
MnO	0.24	0.25	0.29	0.28	0.47	0.31	0.29	0.26	0.31	0.34	0.24
MgO	43.03	42.63	43.91	41.21	35.27	41.25	43.76	40.16	41.28	41.92	42.23
CaO	0.23	0.2	0.19	0.17	0.44	0.26	0.18	0.3	0.24	0.21	0.20
Total	100.00	100.00	100.00	100.00	100.00	100.00	100.00	100.00	100.00	100.00	100.00

Table 2: Microprobe analysis of titanium augites in wt%

Sample No.	1	2	3	4	5	6	7	8	9	10	11
SiO_2	45.72	47.45	49.7	48.72	48.32	46.34	46.74	45.93	42.63	48.07	48.32
TiO_2	3.06	2.74	1.85	2.27	2.51	3.32	2.82	4.16	4.52	2.47	2.51
Al_2O_3	8.09	5.99	4.44	4.78	5.26	7.42	6.77	6.82	10.16	5.66	5.26
Cr_2O_3	0.44	0.21	0.18	0.00	0.00	0.32	0.22	0.00	0.33	0.19	0.00
FeO	7.95	8.21	7.5	8	8.42	7.97	8.51	9.58	8.7	8.21	8.42
MnO	0.00	0.00	0.16	0.25	0.16	0.00	0.00	0.18	0.14	0	0.16
MgO	11.94	12.68	13.81	13.34	13.07	11.96	12.41	10.93	10.57	12.84	13.07
CaO	22.81	22.71	22.35	22.63	22.26	22.76	22.24	21.86	22.65	22.57	22.26
Na_2O	0.00	0.00	0.00	0.00	0.00	0.00	0.003	0.54	0.29	0.00	0.00
Total	100.00	100.00	100.00	100.00	100.00	100.00	100.00	100.00	100.00	100.00	100.00

Table 3: Microprobe analysis of plagioclase in wt%

Sample No.	1	2	3	4	5	6
SiO_2	52.29	53.6	51.92	52.98	52.9	54.63
TiO_2	0.00	0.23	0.00	0.22	0.19	0.17
Al_2O_3	30.12	28.92	30.59	29.49	29.65	28.31
FeO	0.8	0.62	0.59	0.14	0.51	0.15
MnO	0.00	0.00	0.00	0.65	0.00	0.07
MgO	0.00	0.00	0.00	0.00	0.00	0.00
CaO	12.63	11.29	12.92	11.85	12.18	10.19
K_2O	0.18	0.42	0.22	0.31	0.23	0.43
Na_2O	3.97	4.92	3.76	4.35	4.34	5.37
Total	100.0	100.0	100.0	100.0	100.0	100.0

Table 4: Microprobe analysis of magnetites and ilmenites in wt%

Sample No	1	2	3	4	5
SiO_2	0.05	0.05	0.06	0.03	0.06
TiO_2	26.33	25.12	23.06	48.91	47.4
Al_2O_3	2.25	1.74	1.66	0.00	0.07
Cr_2O_3	1.19	1.19	0.23	0.07	0.11
FeO	68.01	68.9	70.93	44.59	46.11
MgO	3.04	2.94	3.8	5.6	6.24
CaO	0.00	0.00	0.00	0.09	0.00
MnO	0.53	0.54	0.48	0.58	0.61
Total	101.4	101.4	100.22	99.87	100.6

1.2.3: Magnetite samples. 4.5: Ilmenite samples.
Fe calculated as FeO.

Table 5a: Chemical analysis of tuff samples in wt%

Sample No.	1	2	3	4	5	6	7	8	9
SiO_2	47.96	46.66	47.19	47.18	49.97	46.21	47.4	47.47	47.9
TiO_2	1.54	1.73	1.56	1.58	1.39	2.13	1.49	1.6	1.30
Al_2O_3	14.61	14.36	14.64	14.21	15.86	14.86	14.77	14.64	14.74
Fe_2O_3	3.04	3.23	3.06	3.08	2.89	3.63	2.99	3.1	2.8
FeO	8.05	8.03	8.37	13.21	8.22	7.8	8.44	8.03	8.42
MnO	0.2	0.22	0.21	0.21	0.21	0.21	0.2	0.2	0.19
MgO	8.85	8.96	9.24	9.34	7.38	9.09	9.09	9.01	9.77
CaO	10.03	10.35	9.89	9.07	7.11	10.1	9.84	0.3	7.8
Na_2O	3.43	3.45	3.35	3.4	1.95	2.74	2.82	2.88	3.27
K_2O	0.9	0.86	0.85	0.84	0.67	0.81	0.8	0.77	0.68
P_2O_5	0.28	0.46	0.28	0.33	0.3	0.3	0.3	0.28	0.28
H_2O	0.37	0.93	0.43	0.37	2.07	1.01	0.93	1.05	1.1
Total	99.26	99.24	99.07	102.82	98.02	98.89	99.07	98.33	98.25
$Mg/Mg+Fe^{+2}$	0.52	0.53	0.52	0.41	0.52	0.54	0.47	0.51	0.52
5b-CIPW norms									
OR	5.38	5.17	5.09	4.85	5.13	4.89	4.82	4.68	4.14
AB	24.45	21.89	23.02	20.53	24.68	23.69	24.32	25.05	28.48
AN	22.06	21.52	22.71	20.53	24.68	26.42	25.76	25.44	24.22
NE	2.65	4.23	3.1	3.88	1.89				
DI-DI	15.24	16.21	14.5	10.12	14.18	13.9	12.51	11.72	7.88
DI-HD	6.09	6.09	5.85	7.39	5.01	4.39	5.27	4.51	3.21
DI	21.33	22.3	20.34	17.51	19.19	18.29	17.78	16.23	11.09
Hy-En						0.36	1.88	4.55	4.87
Hy-Fs						0.13	0.91	2.01	2.27
Hy						0.5	2.79	6.56	7.14
OL-FO	10.67	10.64	11.64	12.63	12.12	11.44	10.79	9.17	11.58
OL-FA	5.39	5.06	5.94	11.66	5.41	4.57	5.74	4.46	5.96
OL	16.06	15.7	17.58	24.28	17.53	16.01	16.53	13.64	17.54
MT	4.46	4.76	4.5	4.36	5.04	5.38	4.42	4.62	4.18
IL	2.96	3.34	3	2.93	3.69	4.13	2.88	3.12	2.54
AP	0.67	1.11	0.67	0.76	0.68	0.73	0.72	0.68	0.68
5c-Trace elements in ppm									
Ba	265	205	420	245	460	260	255	185	165
Rb	10	15	13	8	16	12	15	10	9
Sr	1055	1030	1005	1180	1120	1125	990	1100	755
Cd	10	20	15	5	25	12	18	25	10
Cr	110	105	95	90	110	95	135	95	130
Ni	80	105	70	70	75	80	70	72	65
Ce	55	46	66	25	35	52	54	63	33
Sc	20	26	22	34	20	15	25	27	36
Li	15	12	7	11	9	10	9	11	13

The low variability of SiO_2, Al_2O_3 and CaO indicates homogeneity of the magma (Al-Fugha, 1993). The TiO_2 content ranges between 1.30 and 2.13 wt% and is independent on the amounts of silica, alkalis and alumina. Titanium as shown in Table 5a is considered to be concentrated in magnetite and ilmenite. The trace elements data in Table 5c show relatively minor variations in elements' concentrations. Crystallization processes involving olivine and pyroxene are responsible for the distribution of trace elements in tuff samples.

The primary magma responsible for the formation of this volcanic tuff is believed to be generated by partial melting of upper-mantle material. The primary alkali basaltic magma can be formed by an extremely small degree of melting at a pressure as low as 13 kbar and can fractionate to tholeiitic liquids between 4 and 12 kbar pressure (Mysen and Kushiro, 1977). Basalts may thus be both direct products of mantle partial melting and the differentiation of more primitive picritic partial melts (Wilson, 1989; Rollinson, 1993).

According to Lorenz and Zimanowski (1977), the numerous and widely distributed tuffaceous volcanoes of Jordan are of phreato-magmatic origin. There is a renewal of volcanism along the western margin of Arabian plate at 13 Ma (e.g. Barberi et al., 1979; Tarawneh et al., 2000).

Alkali basaltic magma appears to be generated by smaller degrees of partial melting <20% of enriched sources at a pressure greater than 10 kbar (Wilson, 1989).

Melting experiment on lherzolite shows that primitive basalts, encompassing both tholeiitic and alkaline varieties, represent a continuum of composition produced by a moderate amount of <20% of partial melting (Jaques and Green, 1980).

The thermometer gives a temperature for the formation of single pyroxene ranging from 1022-1083°C (Wells, 1977). The pressure can be estimated using $(Ca/Ca+Fe^{2+}+ Mg)$ against temperature, with a pressure ratio of 5-10 kbar, Fig. (4) (Lindsley, 1983).

The welded pyroclastic rocks in Jabal Aritain volcano NE Jordan basically differ in the degrees of oxidation and devitrification (Malabeh et al., 2003).

Based on prementioned information, Roony et al. (2005) reported that the recent basalts of the Ethiopian rift were produced in a small degree of partial melting peridotite at 15-25 kbar. According to Tayel and Malabeh (2008), Lajjoun basalt produced in 10% degree partial melting for homogenous mantle source. The variation of incompatible elements implies derivation from peridotite source by variable but low degree of melting (<20%).

CONCLUSIONS

Based on the results of this study, the following conclusions can be made on the nature and origin of NE Jordan volcanic tuffs. They originated from alkali basaltic magma which originated in turn by smaller degree of partial melting (<20%). The parental magma is rich in volatiles and witnessed different degrees of fractionation. The mantle material from which tuff magma originated is peridotite in nature as evidenced from incompatible elements.

REFERENCES

Abou Karaki, N. 1987. Synthese et carte seismotectonique des pays de la bordure orientale de la Mediterranee: sismicite du systeme de failles du Jourdain-Mer Morte. Ph.D. thesis, University of Strasbourg (In French).

Al-Fugha, H. 1993. Geochemistry, mineralogy and petrogenesis of NE Jordan basalt. *Dirasat*, Vol. 20B: 95-109. http://Dar.ju.edu.jo/dirasatonline/articles.asp.

Ambraseys, N., Melville, R. and Adams, R. 1994. The seismicity of Egypt, Arabia and the Red Sea: a historical review. Cambridge Univ. Press, 181 p.

Angelier, J. 1979. Determination of the mean principal stresses for a given fault population. *Tectonophysics*, 56,T_{17}- T_{26}.

Angelier, J. 1989. From orientation to magnitudes in palaeostress determination using fault slip data. *J. Struct. Geol.*, 11: 37-50.

Angelier, J. 1991. Inversion directe de recherche 4-D: comparison physique et mathématique de deux méthodes de détermination des tenseurs des paléocontraintes en tectonique de failles. *C. R. Acad. Sc.,* Paris 312 (II): 1213-1218.

Angelier, J. and Mechler, P. 1977. Sur une methode graphique de recherche des contraintes principales egalement utilisable in tectonique et en seismologie: la methode de diedres droits. *Bull. Soc. Geol. Fr.,* 7: 1309-1318.

Badawy, A. and Horvath, F. 1999. Recent stress field of the Sinai sub-plate region. *Tectonophysics*, 304: 385-403.

Barberi, F., P. Capaldi, G. Marinelli, G. Santacroce, M. Treuil and J. Varet. 1979. Recent basaltic volcanism of Jordan and its implication on the geodynamic history of the Dead Sea shear zone. In International Symposium Geodynamic Evol. of the Afro-Arabian Rift System. Academia Nazionale Dei Lincei 47 (Rome), 667-683. http://volcano.si.edu/world/region.cfm?rnum=03&rpage=sources.

Bence, A.E. and A.L. Albee. 1968. Empirical correction factors for the electron microanalysis of silicates and oxides. *Journal of Geology*, 76: 382-403. http://journals.uchicago.edu/jG/home.

Bender, F. 1968. The geology of Jordan, Bornträger, Berlin, 230 p. http://worldcat.org/oclc/1109639-72k.

Bender, F. 1974. Geology of Jordan, Gebrüder Bornträger Verlag, Berlin, 196 p.

Ben-Menahem, A. 1979. Earthquake catalogue for the Middle East (92BC-AD 1980). *Boll. Geofis. Teorica ed Appl.,* 21: 245-310.

Bott, M.H.P. 1959. The mechanism of oblique slip faulting. *Geological Magazine*, 96: 109-117.

Camp, V. E. and Roobol, M. J. 1989. The Arabian continental alkali basalt province: Part 1. Evolution Harrat Rahat, Kingdom of Saudi Arabia, *Geol. Soc. Amer. Bull.,* 101: 71-95.

Delvaux, D. 1993. The TENSOR program for reconstruction: examples from the east Africa and the Baikal Rift systems. *Terra Abstr., Abstr. Suppl. Terra Nova,* 5: 216.

Delvaux, D., Moeys, R., Stapel, G., Petit, C., Levi, K., Miroshnichenko, A., Ruzhich, V. and Sankov, V. 1997. Paleostress reconstructions and geodynamics of the Baikal region, Central Asia, Part 2. Cenozoic rifting. *Tectonophysics*, 282: 1-38.

Diabat, A. 1999. Paleostress and strain analysis of the Cretaceous rocks in the eastern margin of the Dead Sea transform, Jordan. Ph.D. Thesis, Baghdad University, Iraq.

Diabat, A., Atallah, M. and Salih, M. 2004. Paleostress analysis of the Cretaceous rocks in the eastern margin of the Dead Sea transform. *Journal of African Earth Sciences*, 38: 449-460.

Duffield, W., Mc Kee, El-Salem, F. and Feimeh, M. 1988. K-Ar ages, chemical composition and geothermal significance of Cenozoic basalt near the Jordan Rift, *Geothermics*, 17: 635-644.

Eyal, Y. 1996. Stress fluctuations along the Dead Sea rift since the Middle Miocene. *Tectonics*, 15: 157-170.

Eyal, Y. and Reches, Z. 1983. Tectonic analysis of the Dead Sea rift region since the Late Cretaceous based on mesostructures. *Tectonics*, 2: 167-185.

Eyal, Y. 1985. Intraplate deformation by block rotation and mesostructures along the Dead Sea transform, northern

Israel. *Tectonics*, 4: 85-105.

Fediuk, F. and Al-Fugha, H. 1999. Dead Sea region fault-controlled chemistry of Cenozoic volcanics. *Geolines Praha*, 9: 29-34. http://geolines.gli.cas.cz/fileadmin/volumes.

Freund, R., Garfunkel, Z., Zak, J., Goldberg, M., Weissbrod, T. and Derin, B. 1970. The shear along the Dead Sea rift. Royal Soc. Lond., *Phil. Trans.,* A267: 107-130.

Galli, P. 1999. Active tectonics along the Wadi Araba-Jordan Valley transform fault, *Geophysical Research*, 104: 2777-2796.

Garfunkel, Z. 1981. Internal structure of the Dead Sea leaky transform (rift) in relation to plate kinematics. *Tectonophysics*, 80: 81-108.

Garfunkel, Z., Zak, I. and Freund, R. 1981. Active faulting in the Dead Sea rift. *Tectonphysics*, 80: 1-26.

Ibrahim, K. M. 1993. The geological framework for the Harrat Asham basalt super-group and its volcanotectonic evolution. Natural Resources Authority (NRA), *Geol. Map. Div.,* 25, 33p.

Ibrahim, K. M. 1996. The regional geology of Al-Azraq area. Natural Resources Authority (NRA), *Geol. Map. Div.,* 36, 67p.

Ibrahim, K. and Al-Malabeh, A. 2006. Geochemistry and volcanic features of Harrat El-Fahda, a young volcanic field in northwest Arabia, Jordan, *Journal of Asian Sciences*, 127 (2): 127-154.

Ilani, S., Harlavn, Y., Tarawneh, K., Rabba, I., Weinberger, R., Ibrahim, K. M., Peltz, S. and Steinitz, G. 2001. New K-Ar ages of basalts from the Harrat Ash Shaam volcanic field in Jordan: implication for the span and duration of the upper mantle upwelling beneath the western Arabian plate, *Geology*, 29: 171-174.

Jaques, A.L. and D.H. Green. 1980. Anhydrous melting of peridotite at 0-15 kbar pressure and the genesis of tholeiitic basalt contrib. *Mineral Petrol.*, 73: 287-310. http://springerlink.com/content/100406.

Lindsley, D.H. 1983. Pyroxene thermometry. *Am. Mineral.*, 68: 477-493. http://minsocam/MSA/AmMin/Toc.

Lorenz, V. and Zimanowski, B. 1977. Variation of coexisting phases with degree of melting of an upper mantle. *Am. Mineral.,* 62: 843-865. http://minsocam/MSA/AmMin/Toc.

Malabeh, A. 2003. Geochemistry and volcaology of Jabal Al-Rufiyat, stromblian monogenic volcano, Jordan, *Dirasat*, 30: 125-140.

Malabeh, A. Al-Fugha and T. El-Hassan. 2003. Volcano genesis of welded pyroclastic Rocks in Jabal Aritain volcano, Jordan. *Abhath-Alyarmouk*, Yarmouk Univ., 12: 345-361.

Malabeh, A. 1994. Geochemistry of two volcanic cones from the intra-continental plateau basalt of Hara El-Jabban, NE-Jordan, *Geochemical Journal*, 28: 517-540.

Malabeh, A., El-Hasan, T., Lataifeh, M. and OShea, M. 2002. Geochemical and mineralogical related magnetic characteristic of the Tertiary-Quaternary (Umm Al-Qutein) basaltic flows from the basaltic field of Harra El-Jabban, northeast Jordan, *Physics of Condensed Matter*, Netherlands, 321 (1-4): 396-403.

Moffat, D. 1988. A volcano tectonic analysis of the Cenozoic continental basalts of northern Jordan: implication for hydrocarbon prospectively in the block B area, Unpubl. Report, University College of Swansen, UK.

Mysen, B.O. and R. Kushiro. 1977. Compositional variation of coexisting phases with degree of melting of peridotite in upper mantle. *Am. Mineral.*, 62: 843-865. http://minsocam/MSA/AmMin/Toc.

Niemi, T.M., Zhang, H., Atallah, M. and Harrison, B.J. 2001. Late Pleistocene and Holocene slip rate of the northern Wadi Araba fault, Dead Sea Transform, Jordan. *Journal of Seismology*, 5: 449-474.

Picard, L. 1943. Structure and evolution of Palestine. *Bull. of Geology Department*, Hebrew University, Jerusalem, Palestine, 4: 135pp.

Quennel , A. M. 1958. The structure and geomorphic evolution of the Dead Sea rift. *Quart. J. Geol. Soc. Lond.*, 114: 1-24.

Rollinson, H. 1993. Using geochemical data; evolution, presentation, interpretation. Longman Scientific and Technical, Essex, 352 p.

Roony, T., T. Furman, G. Yirgu and D. Ayalew. 2005. Structure of the Ethiopian lithosphere: Xenolith evidence in the main Ethiopian rift. *Geochimica et Cosmochica Acta*, 69: 3889-3910. http://sciencedirect. com/science.?-ob=article.

Saffarini, G., Nassir, S. and Abed, A. 1985. A contribution to the petrology and geochemistry of the Quaternary-Neogene basalts of central Jordan, *Dirasat*, 12: 133-144.

Shaw, J., Baker, J., Menzies, M., Thirlwall, B. and Ibrahim, K. 2003. Petrogensis of the largest interaplate volcanic field on the Arabian plate (Jordan): a mixed lithosphere-asthenosphere source activated by lithosphere extension, *J. Petrol.*, 44 (9): 1657-1679.

Tarawneh, K. 1999a. Wadi al-Abid geological map, scale 1:50,000, NRA, Geol. Map. Div., Amman.

Tarawneh, K. 1999b. The geology of Wadi al-Abid area, NRA, *Geol. Map. Div. Bull.*, 44: 12-14.

Tarawneh, K., Ilani, S., Rabba, I., Harlavan, Y., Peltz, S.,

Ibrahim, K., Weinberger, R. and Steinitz, G. 2000. Dating of the Harrat Ashaam basalts northeast Jordan (phase 1). Natural Resources Authority and Geological Survey of Israel, *Report GSI.2,* 58 p.

Tayel El-Hasan and Ahmad Al-Malabeh. 2008. Geochemistry, mineralogy and petrogenesis of El-Lajjoun Pleistocene alkali basalt of central Jordan. *Jordan Journal of Earth and Environmental Sciences*, 1 (2): 53-62.

Wells, P.R.A. 1977. Pyroxene thermometry in simple and complex systems. *Contrib. Mineral. Petrol.*, 62: 129-139. http://springerlink.com/content/100406.

Wilson, M. 1989. Igneous petrogenesis, a global tectonic approach.1st Edn., Unwin, London, 466.

Zain Eldeen, U., Delvaux, D. and Jacobs, P. 2002. Tectonic evolution in the Wadi Araba segment of the Dead Sea rift, southwest Jordan. *EUG Stephan Mueller Special Publication Series*, 2: 63-81.